eppendorf

eBook on Bioprocessing Basics

Bioreactors are more than just vessels! Do you want to learn more about the key characteristics of a bioreactor and the differences between batch, fed-batch, and continuous fermentation modes? Then download our eBook in which we provide information on the basics of bioprocessing.

Get your free copy now!
https://eppendorf.group/bioprocessing-basics

Eppendorf® and the Eppendorf Brand Design are registered trademarks of Eppendorf SE, Germany.
All rights reserved, including graphics and images. Copyright © 2022 by Eppendorf SE.

www.eppendorf.com/bioprocess-basics

Check for updates

Received: 16 April 2021 | Revised: 19 September 2021 | Accepted: 4 October 2021

DOI: 10.1002/bit.27966

ARTICLE

BIOTECHNOLOGY BIOENGINEERING WILEY

Salicylic acid inducible nucleocytoplasmic shuttling of NPR1 fusion proteins in human cells

Fatemeh Sadeghi[1] | Monish Kumar[1] | Irfan N. Bandey[1] | Xiaoyang Li[2] | Badrinath Roysam[2] | Navin Varadarajan[1]

[1]Department of Chemical and Biomolecular Engineering, University of Houston, Houston, Texas, USA

[2]Department of Electrical and Computer Engineering, University of Houston, Houston, Texas, USA

Correspondence

Navin Varadarajan, Department of Chemical and Biomolecular Engineering, University of Houston, Houston, TX 77004, USA.
Email: nvaradar@central.uh.edu

Funding information

MRA Established Investigator Award, Grant/Award Number: 509800; CDMRP, Grant/Award Number: CA160591; Cancer Prevention and Research Institute of Texas, Grant/Award Number: RP180466; Owens foundation; NIH, Grant/Award Numbers: U01AI148118, R01GM143243; NSF, Grant/Award Number: 1705464

Abstract

Ligand inducible proteins that enable precise and reversible control of nuclear translocation of passenger proteins have broad applications ranging from genetic studies in mammals to therapeutics that target diseases such as cancer and diabetes. One of the drawbacks of the current translocation systems is that the ligands used to control nuclear localization are either toxic or prone to crosstalk with endogenous protein cascades within live animals. We sought to take advantage of salicylic acid (SA), a small molecule that has been extensively used in humans. In plants, SA functions as a hormone that can mediate immunity and is sensed by the non-expressor of pathogenesis-related (NPR) proteins. Although it is well recognized that nuclear translocation of NPR1 is essential to promoting immunity in plants, the exact subdomain of *Arabidopsis thaliana* NPR1 (AtNPR1) essential for SA-mediated nuclear translocation is controversial. Here, we utilized the fluorescent protein mCherry as the reporter to investigate the ability of SA to induce nuclear translocation of the full-length NPR1 protein or its C-terminal transactivation (TAD) domain using HEK293 cells as a heterologous system. HEK293 cells lack accessory plant proteins including NPR3/NPR4 and are thus ideally suited for studying the impact of SA-induced changes in NPR1. Our results obtained using a stable expression system show that the TAD of AtNPR1 is sufficient to enable the reversible SA-mediated nuclear translocation of mCherry. Our studies advance a basic understanding of nuclear translocation mediated by the TAD of AtNPR1 and uncover a biotechnological tool for SA-mediated nuclear localization.

KEYWORDS

nuclear translocation, plants, salicylic acid, synthetic biology

1 | INTRODUCTION

Inducible control of nuclear localization is a fundamental mechanism naturally employed by cells to enable posttranscriptional control of cellular function and fate. At the molecular level, the change in protein localization is typically facilitated by a change in protein conformation upon ligand binding that exposes a nuclear localization signal (NLS), enabling transport to the nucleus. Identifying proteins or their subdomains responsible for the nucleocytoplasmic shuttling in a ligand-dependent manner has provided tools for diverse applications: (a) basic biology: conditional knockout to study gene functions in specific tissues by fusion to the Cre recombinase (Feil et al., 1996);

Fatemeh Sadeghi and Monish Kumar contributed equally to this study.

 © 2021 Wiley Periodicals LLC

10970290, 2022, 1, Downloaded from https://onlinelibrary.wiley.com/doi/10.1002/bit.27966 by University Of Houston Library Central Campus, Wiley Online Library on [12/02/2023]. See the Terms and Conditions (https://onlinelibrary.wiley.com/terms-and-conditions) on Wiley Online Library for rules of use; OA articles are governed by the applicable Creative Commons License

(b) synthetic biology: inducible CRISPR/Cas9 switches for transcriptional activation and genome editing (Zhang et al., 2019; Zhao et al., 2018); and (c) cell therapies: inducible apoptosis to eliminate therapeutic cells on demand (Liu et al., 2018). Two major systems have been widely utilized to control the inducible translocation of proteins of interest: (a) the estrogen receptor and its ligand tamoxifen (Feil et al., 1996; Fuhrmann-Benzakein et al., 2000), and (b) rapamycin-induced dimerization of the FK506 binding protein (FKBP) and the FKBP12-rapamycin-binding (FRB) domain of mammalian target of rapamycin (mTOR; Liu et al., 2018; Xu et al., 2010). These systems are however not without their drawbacks especially for therapeutic applications; tamoxifen, as an estrogen modulator has an impact on cells throughout the body, and rapamycin (and its analogs, rapalogs), can have a direct impact on the essential mTOR pathway in multiple cell types (Di Ventura & Kuhlman, 2016). We sought to identify protein or protein subdomains that can facilitate inducible nuclear translocation in response to small molecules well studied for administration to mammals/humans.

Salicylic acid (SA), derived from plants, has been used medicinally in humans since antiquity. This extensive history of the safety of human use of SA prompted us to investigate proteins or subdomains that can enable nucleocytoplasmic shuttling in response to SA. Within plants, SA is a hormone that plays a key role in innate immunity via the induction of systemic acquired resistance (SAR). Studies suggest that pathogen infection results in the accumulation of SA in infected tissues and distal leaves of the plant and this precedes the upregulation of pathogenesis-related genes (PR genes; Malamy et al., 1990; Métraux et al., 1990; Tsuda et al., 2009). In *Arabidopsis thaliana*, both the nonexpressor of PR genes 1 (NPR1) protein and NPR3/4 proteins function as SA receptors (Fu et al., 2012; Wu et al., 2012). NPR1 functions as a transcriptional co-activator whereas NPR3/4 function as transcriptional co-repressors of the expression of genes associated with plant immunity (Ding et al., 2018). Although the function of NPR1/3/4 as SA receptors is established, the exact nature and outcome of the molecular interaction between NPR1 and SA remain controversial. Many different roles have been proposed for this interaction between SA and NPR1 including influencing the oligomerization state, nuclear translocation, and promoting the interaction between NPR1 and NPR3/4 (Kinkema et al., 2000; Rochon et al., 2006; Tada et al., 2008).

In this study, we utilized the fluorescent protein mCherry as the reporter to investigate the ability of SA to induce nuclear translocation of the full-length NPR1 protein or its C-terminal transactivation (TAD) domain using a heterologous system. Our rationale for using the mammalian expression system, HEK293 cells, was that all the other accessory proteins including NPR3/NPR4 are absent in these cells, and is thus ideally suited for directly studying the impact of SA induced conformation changes in NPR1. Our results illustrate that the C-terminal TAD of NPR1 is sufficient to enable the SA-mediated nuclear translocation of mCherry. Systematic analyses show that fusion proteins containing either full-length NPR1 or NPR1-TAD are capable of nuclear translocation in response to SA. The response to SA is reversible and the proteins revert to their basal localization upon withdrawal of SA. Our studies advance a basic understanding of nuclear translocation mediated by the TAD of NPR1 and provide a biotechnological tool for ligand-induced reversible nuclear localization.

2 | EXPERIMENTAL METHODS

2.1 | Molecular cloning using pcDNA3.4 vector

We obtained the gene fragments coding for mCherry, mCherry-NLS, and mCherry-NPR1-TAD by PCR. For the construction of the mCherry-NLS, the NLS sequence from the simian vacuolating virus (SV40) was fused to the mCherry gene at the C-terminus. The gene fragment coding for NPR1 was purchased from Integrated DNA Technologies. The plasmid containing the mCherry gene was a kind gift from Dr. Xinping Fu (University of Houston). We amplified the gene encoding mCherry-NPR1-TAD by PCR using primers designed to encode a His_8 tag (3′), in addition to the restriction enzyme recognition sites (5′ and 3′). Primers for mCherry and mCherry-NLS constructs were designed without the His_8 tag. Genetic fusion of mCherry to NPR1-TAD was accomplished via overlap extension PCR (OE-PCR). We digested the PCR products and pcDNA3.4 using Bsu36I-HF and AgeI-HF at 37°C for 3 h and ligated them using T4 DNA ligase at 16°C overnight. We transformed the plasmids into *Escherichia coli* MC1061 cells by electroporation and verified the sequences by standard Sanger sequencing (Genewiz). Next, single colonies for each of the mCherry, mCherry-NLS, and mCherry-NPR1-TAD constructs were inoculated in 100 ml of Lysogeny broth (LB) medium supplemented with 200 μg/ml ampicillin in separate flasks. We grew the cells at 37°C overnight in an orbital shaker. Plasmid DNAs were isolated using QIAGEN Plasmid Maxi Kit and QIAvac 24 Plus Vacuum Manifold (Qiagen Inc.).

2.2 | Molecular cloning using dCAS9_VP64_GFP lentiviral backbone

We used Gibson assembly for the cloning of the constructs mCherry-NPR1-TAD, NPR1-TAD-mCherry, mCherry-linker-NPR1, and NPR1-linker-mCherry using the backbone of dCAS9_VP64 _GFP (Addgene, plasmid #61422). The linker used in these constructs was $(SGGG)_1(SGGGG)_2$. The constructs were transformed by heat shock into *E. coli* E cloni chemical competent cells following the protocol described by the manufacturer (Lucigen). We isolated the plasmids and confirmed their sequence by Sanger sequencing.

2.3 | Transfection into HEK293T cells

We used low-passage HEK293T cells with greater than 90% viability for transient transfection of the plasmid constructs using Lipofectamine LTX reagent (Thermo Fisher Scientific). The cells were trypsinized and counted using trypan blue (STEMCELL

10970290, 2022, 1, Downloaded from https://onlinelibrary.wiley.com/doi/10.1002/bit.27966 by University Of Houston Library Central Campus, Wiley Online Library on [12/02/2023]. See the Terms and Conditions (https://onlinelibrary.wiley.com/terms-and-conditions) on Wiley Online Library for rules of use; OA articles are governed by the applicable Creative Commons License

Technologies). 5×10^5 cells were seeded into a six-well plate, the day before transfection in 3 ml R10 (RPMI-1640 supplemented with 10% fetal bovine serum and L-glutamine) growth medium to 50%–80% confluency. On the day of transfection, 2 µg of the plasmid along with 2 µl PLUS reagent from the Lipofectamine LTX Transfection Kit (Invitrogen) was added to 200 µl of the opti-MEM media (Invitrogen). Next, 4 µl of the Lipofectamine LTX reagent was diluted in 200 µl of the same media, and each reaction mix was incubated separately. After 5 min, the two tube contents were mixed to allow the DNA-Lipofectamine complex to form. After 30 min of incubation, the mixture was added to the cells, and 4 h later the media was replaced with 3 ml of fresh R10.

2.4 | Generation of the stable cell line

5×10^6 of HEK293 cells were seeded into a T25 flask with 5 mL DMEM F12 media the day before transfection. On the day of transfection, 6 µg of the target plasmid, 5 µg of the psPAX plasmid, and 3 µg of the MD2G plasmid were transfected into HEK293 cells using Lipofectamine transfection protocol. One day after transfection, the media was removed and replaced with 10 ml of fresh R10 medium. We harvested the supernatant from the cells after 72 h and concentrated the supernatants using Amicon Ultra-15 filters. These viral particles were used to infect 6×10^6 HEK293 cells. Next, the mCherry-expressing HEK293 cells were sorted (FACSAria Fusion, MDACC) 1 week after transduction. Sorted cells were propagated using R10 medium, and used for subsequent experiments.

2.5 | Staining and microscopy

Cells expressing the protein of interest were harvested by spinning down at 350*g* for 5 min and washed with 1× phosphate-buffered saline (PBS) three times. 1×10^6 cells were resuspended in 1 ml of 1× PBS, and 10 µg/ml of the Hoechst 33342 dye (Thermo Fisher Scientific) was added to the cells and incubated at 37°C for 20 min. Next, 4×10^5 cells were loaded into a 35-mm petri dish, and mCherry-positive cells were imaged using a 100× (oil) 1.49 NA objective on A1/TiE inverted confocal microscope (Nikon Instruments Inc.). Image analysis was performed on at least thirty cells that were positive for both mCherry protein and Hoechst dye. N/C/D analysis was performed by visualization. Translocation was considered to be "predominantly in the nucleus"(N) if no mCherry signal was seen in other cellular compartments. The same decision-making trend was applied to "predominantly in the cytoplasm"(C) and "distributed all over the cell"(D) conditions. To track the localization of single-cells, we loaded 100 µl of stained cells at a density of 1×10^6/ml into a micromesh array with a 50-µm depth size (microsurfaces). The Pearson's co-localization coefficient was calculated using JaCop plugin on ImageJ.

2.6 | SA dose optimization assay

SA was added to cells at final concentrations of 1 µM, 10 µM, 100 µM, 500 µM, 1 mM, and 2.5 mM. Cells were imaged before addition of SA and 24 h after addition of SA. The relative change on average PCC at different concentrations with respect to no addition of SA was calculated using the formula $(X_c - X_0) \pm \sqrt{\left(\mathrm{SEM}_c^2 + \mathrm{SEM}_0^2\right)}$, where X_C and X_0 are mean PCC values and SEM_C and SEM_0 are corresponding standard error of the mean(SEM) at SA concentration C and 0, respectively. The relative change in PCC was plotted against SA concentration and linear regression was performed in Graphpad Prism.

2.7 | Reversibility assay

We recorded an initial image of the cells in the absence of SA. Next, we added SA at a final concentration of 2.5 mM, and the reversibility potential of the NPR1 variants was determined by monitoring the co-localization for up to 30 h after the addition of SA. At this time, the media containing SA was carefully decanted and replaced with fresh R10 media. The cells were placed in the incubator for 18 more hours (48 h from time zero) and images were captured using a confocal microscope.

2.8 | Structure prediction of AtNPR1

The structure of AtNPR1 was predicted using the Phyre2 web portal for protein modeling, prediction, and analysis (Kelley et al., 2015). The predicted model was visualized and edited using the EzMol interface (Reynolds et al., 2018).

3 | RESULTS

3.1 | NPR1-TAD is sufficient for translocation of mCherry

To establish controls and determine the dynamic range for nuclear localization, we cloned mCherry and mCherry fused to a C-terminal NLS (mCherry-NLS) into a pcDNA based plasmid. The plasmids were individually transfected into HEK293 cells (Figure 1a). The cells were stained with the nuclear stain, DAPI, and visualized by fluorescent confocal microscopy (Figure 1b). We quantified the degree of localization by subcategorizing cells expressing cargo mCherry as N (predominantly in the nucleus), C (predominantly in the cytoplasm), and D (distributed all over the cell). As expected, 97% of HEK293 cells transfected with mCherry showed diffuse staining indicating that the protein was present both in the cytoplasm and the nucleus (Figure 1b,d). By contrast, 52% of cells transfected with mCherry-NLS showed predominant nuclear localization (Figure 1b,d). We quantified

10970290, 2022, 1, Downloaded from https://onlinelibrary.wiley.com/doi/10.1002/bit.27966 by University Of Houston Library Central Campus, Wiley Online Library on [12/02/2023]. See the Terms and Conditions (https://onlinelibrary.wiley.com/terms-and-conditions) on Wiley Online Library for rules of use; OA articles are governed by the applicable Creative Commons License

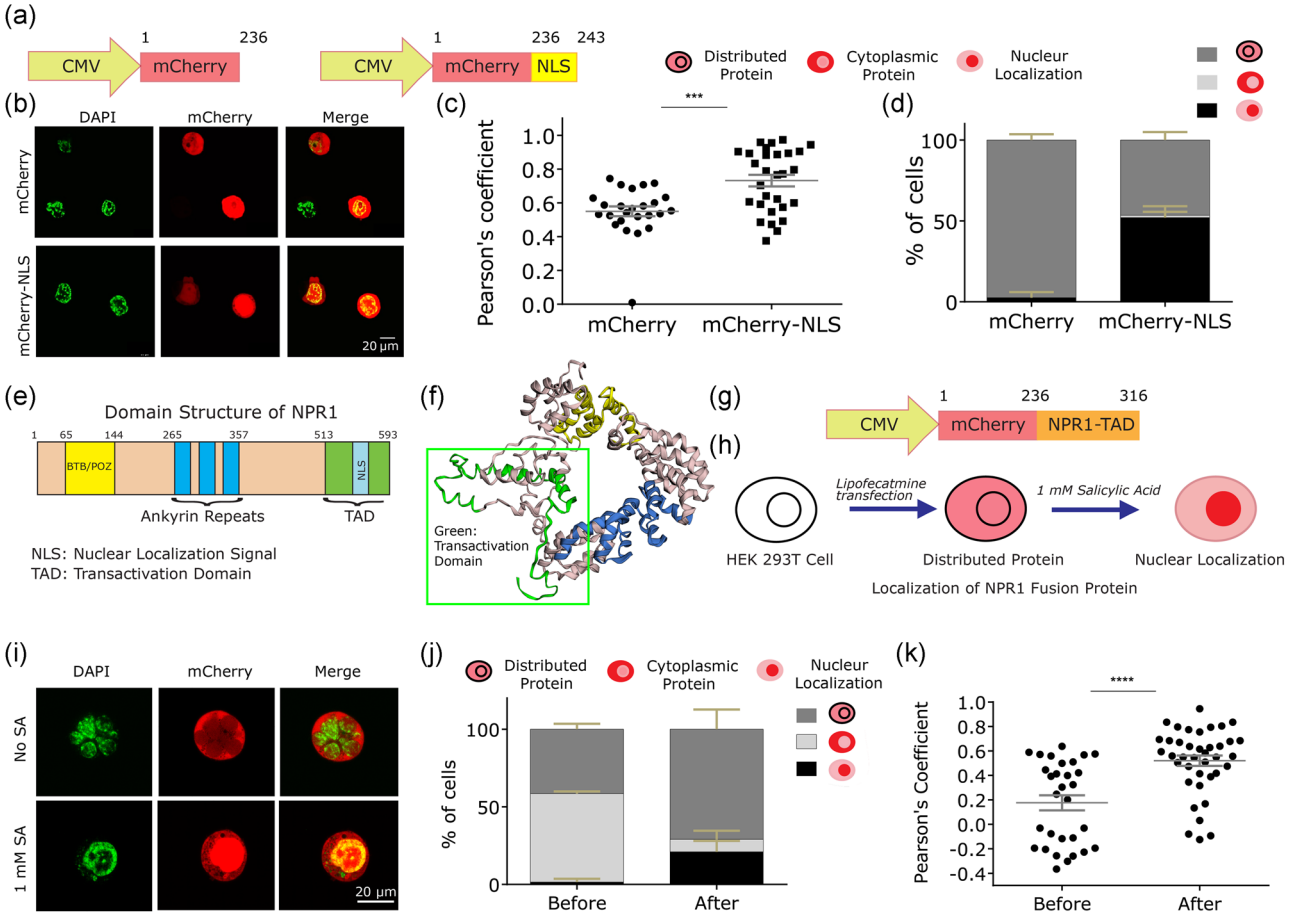

FIGURE 1 Fusion to NPR1-TAD facilitates translocation of the mCherry reporter protein. (a) Constructs depicting mCherry and mCherry-NLS under CMV promoter in a pcDNA-based vector. (b) Microscopy images representing intracellular localization of mCherry and mCherry-NLS. HEK 293T cells were stained with DAPI after transient transfection with mCherry and mCherry-NLS. mCherry-NLS protein is significantly localized in the nucleus as opposed to the more diffuse mCherry protein as indicated by (c) PCC and (d) Percentage of N, C, and D distributions. At least 30 single cells from one of three representative experiments are shown. A t-test was used for comparing the two distributions. ***$p < 0.001$. (e) Domain architecture of NPR1 illustrates that the NLS is incorporated in the C-terminal TAD domain. (f) The modeled structure of the NPR1 predicts six helix bundles in the full-length protein. (g) The design strategy of pcDNA-based plasmid vector expressing NPR1-TAD under CMV promoter for transient transfection experiments. (h) Work-flow showing SA-induced protein translocation after transient expression in HEK 293T mammalian cells. (i) Representative confocal microscopy images of DAPI (nucleus), mCherry, and the merged channels showing an increased diffuse expression of mCherry after SA treatment. (j) Bargraph illustrating the percentage of cells with nuclear (N), cytoplasmic (C), or distributed (D) protein. Treatment of mCherry-NPR1-TAD with SA altered the behavior of this fusion protein from predominantly cytoplasmic to diffuse localization. The error bars represent the SEM of three independent trials. (k) Pearson's coefficients were computed for mCherry-NPR1-TAD in the absence and presence of SA confirming its SA-dependent translocation. The error bars represent the SEM. At least 30 single cells from one of three representative experiments are shown. A *t*-test was used for comparing the two distributions. $p < 0.0001$

the degree of nuclear co-localization by computing Pearson's correlation coefficient (PCC; Figure 1c). PCC values close to one imply nuclear localization of mCherry while a value close to −1 implies nuclear exclusion of mCherry (Figure S2). These results also confirmed that cells expressing mCherry-NLS showed an enrichment of the protein in the nucleus compared to cells expressing mCherry.

It has been proposed that the TAD domain of *A. thaliana* NPR1 (AtNPR1), amino acids 513–593, harbors the SA-binding domain and the NLS fragment (Figure 1e; Wu et al., 2012). The NLS is of AtNPR1 is an 18-aa long peptide located in between amino acids 537–554 with the complete sequence of KRLQKKQRYMEIQETLKK (UniProtKB-P93002 [NPR1-ARATH]). Although the structure of AtNPR1 is not available, the predicted structure based on modeling indicated that NPR1 comprises sets of helix bundles and that the TAD is a part of one such bundle (Figure 1f). We thus hypothesized that the NPR1-TAD is sufficient for the ligand-induced nuclear translocation of passenger proteins. We tested this hypothesis using a heterologous expression platform in mammalian cells with the reasoning that any other plant-specific, NPR1 associated accessory proteins needed for translocation are absent in mammalian cells. Accordingly, we cloned the mCherry-NPR1-TAD fusion protein into the same

10970290, 2022, 1, Downloaded from https://onlinelibrary.wiley.com/doi/10.1002/bit.27966 by University Of Houston Library Central Campus, Wiley Online Library on [12/02/2023]. See the Terms and Conditions (https://onlinelibrary.wiley.com/terms-and-conditions) on Wiley Online Library for rules of use; OA articles are governed by the applicable Creative Commons License

pcDNA backbone (Figure 1g). We transiently transfected the plasmid into HEK293 cells and imaged the localization of mCherry before and after the addition of 1 mM SA (Wu et al., 2012; Figure 1h). In the absence of SA, 57% of the cells expressing mCherry-NPR1-TAD showed predominant cytoplasmic staining (Figure 1i,j). Twenty-four hours after the addition of 1 mM SA, only 8% of cells showed predominant cytoplasmic staining (Figure 1i,j). This change was also reflected in the nuclear localization of the proteins within the same cells. The frequency of cells expressing mCherry in the nucleus (D & N staining) increased from 43% to 92% (Figure 1j). We quantified the overlap of the mCherry signal with the nuclear stain using PCC. Consistent with the subcellular classification, 57% of the cells showed a negative correlation in the absence of SA, indicative of cytoplasmic expression. In the presence of SA 92% of cells showed a significant nuclear correlation (Figure 1k; 0.18 ± 0.03 vs. 0.56 ± 0.09, $p < 0.0001$). Collectively, these results using transient transfections, established that the NPR1-TAD is sufficient for SA-induced nuclear translocation of mCherry in human cells. The magnitude of cells with increased nuclear localization upon the addition of ligand compares favorably to the tamoxifen inducible estrogen receptor alpha system (Zhao et al., 2018).

3.2 | Differential subcellular localization of NPR1 fusion proteins

In our initial experiments, we fused the NPR1-TAD at the C-terminus of mCherry since this is consistent with the localization of TAD within NPR1. Having established that the NPR1-TAD can mediate the nuclear translocation of mCherry, our next aim was to systematically investigate whether (a) TAD can function at both N and C termini, and (b) if the translocation mediated by full-length NPR1 behaved differently to the translocation mediated by the NPR1-TAD. Accordingly, we designed four separate constructs with mCherry as the reporter protein: mCherry-NPR1-TAD, NPR1-TAD-mCherry, mCherry-NPR1, and NPR1-mCherry (Figure 2a). Flexible Glycine-Serine linkers were inserted in constructs harboring full-length NPR1 to allow for the mobility of the connecting domains (Chen et al., 2013). We cloned the constructs downstream of the EF-1α promoter, transduced them into HEK293 cells, and flow-sorted based on mCherry fluorescence to generate stable cell lines (Figure 2b,c).

To study potential nucleocytoplasmic shuttling, we quantified the localization of mCherry in these stable cell lines in the presence and absence of SA using confocal microscopy. As a control, we cultured the cells without addition of SA for 24 h and verified that the

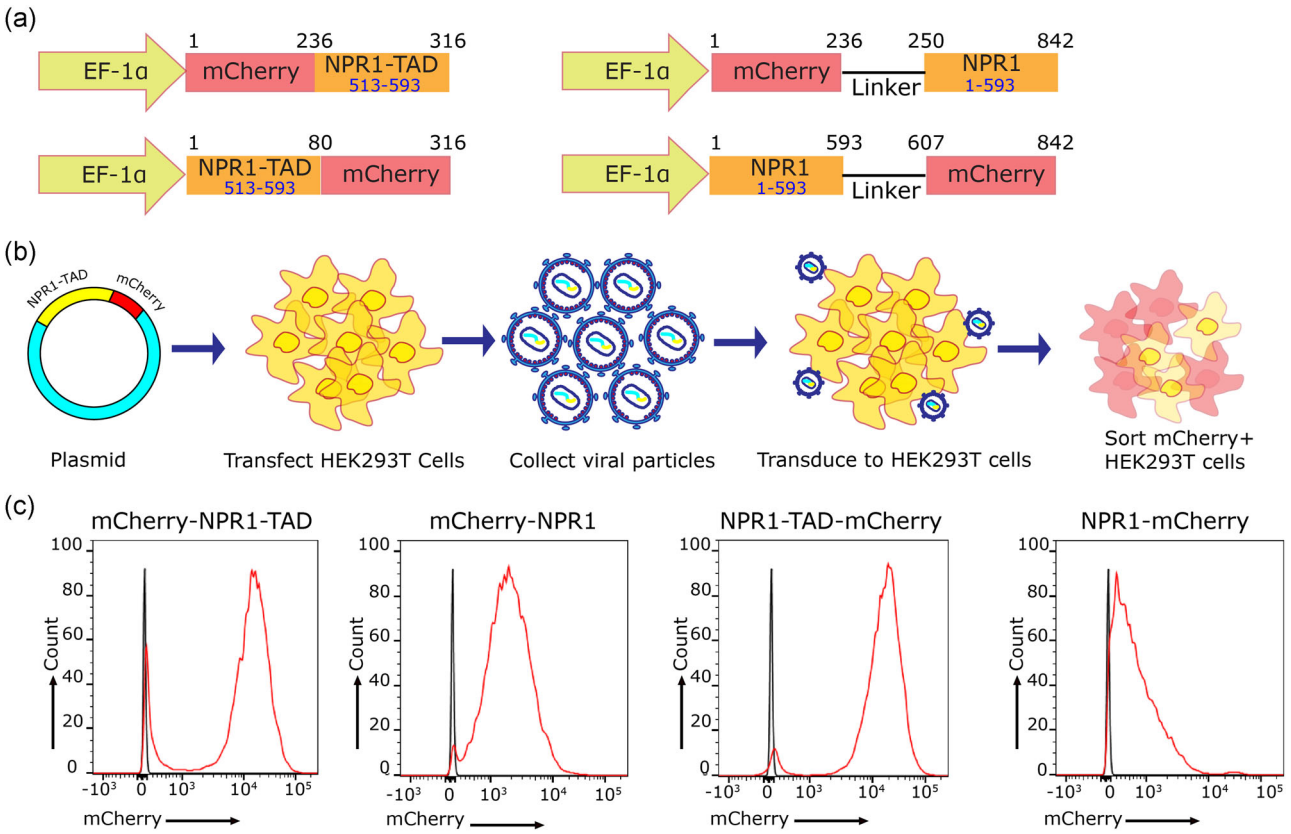

FIGURE 2 Generation of stable mCherry NPR1 fusion proteins in HEK 293T cells. (a) Schematics of the constructs designed for stable expression of mCherry-NPR1-TAD, mCherry-Linker-NPR1, NPR1-TAD-mCherry, and NPR1-Linker-mCherry under EF-1α promoter. (b) Stable expression of NPR1 fusion proteins was obtained by lentiviral transduction of HEK 293T cells. The infected cells were collected and sorted for the cells containing mCherry fluorescent protein. (c) Representative histograms confirming successful stable transfection of the NPR1 proteins (red line) versus the uninfected HEK 293T cells (black line)

10970290, 2022, 1, Downloaded from https://onlinelibrary.wiley.com/doi/10.1002/bit.27966 by University Of Houston Library Central Campus, Wiley Online Library on [12/02/2023]. See the Terms and Conditions (https://onlinelibrary.wiley.com/terms-and-conditions) on Wiley Online Library for rules of use; OA articles are governed by the applicable Creative Commons License

localization of mCherry was invariant with time (Figure S3). Next, we performed SA dose optimization studies for cells stably expressing mCherry-NPR1-TAD, NPR1-TAD-mCherry, and NPR1-mCherry at concentrations varying from 1 μM to 2.5 mM. We observed a linear correlation between increase on average PCC values and SA concentration for all three constructs (Figure S4). Although we used SA at 1 mM concentration in transient transfection experiments, we increased the final SA concentration to 2.5 mM based on our dose optimization experiments (Figure S4). Consistent with the data we obtained with transient transfections, only 4% of cells expressing mCherry-NPR1-TAD showed nuclear localization (D & N) in the absence of SA (Figure 3a,d,g). Upon the addition of SA, 32% of cells showed nuclear localization of mCherry (Figure 3d) and this was also reflected in significant increase in nuclear colocalization by PCC (−0.26 ± 0.04 vs. −0.06 ± 0.01; $p = 0.006$). By comparison, 24% of HEK293 cells expressing the construct with full-length NPR1 at the C-terminus, mCherry-NPR1, showed nuclear localization (D & N) in the absence of SA (Figure S1) and this number was unaltered by the addition of SA (Figure S1b). PCC was also consistent with a lack of change in protein localization in these cells upon the addition of SA (Figure S1c; −0.03 ± 0.01 vs. −0.08 ± 0.02). Collectively these results showed that while both NPR1 and NPR1-TAD when fused to the C-terminus of mCherry facilitate efficient nuclear exclusion, only NPR1-TAD is capable of nuclear translocation in the presence of SA.

We next investigated the two constructs with NPR1 domains at the N-terminus. HEK293 cells expressing NPR1-TAD-mCherry showed a different distribution of mCherry proteins compared to mCherry-NPR1-TAD. 100% of the cells showed nuclear expression (D & N) of mCherry in the presence or absence of SA (Figure 3b,e,h). 47% of the cells had predominant nuclear localization in the absence of SA and the addition of SA increased this frequency to 73%. Thus, the frequency of cells showing only nuclear localization of mCherry increased in the presence of SA and this also led to the significantly increased nuclear colocalization by PCC (0.67 ± 0.11 vs. 0.77 ± 0.14;

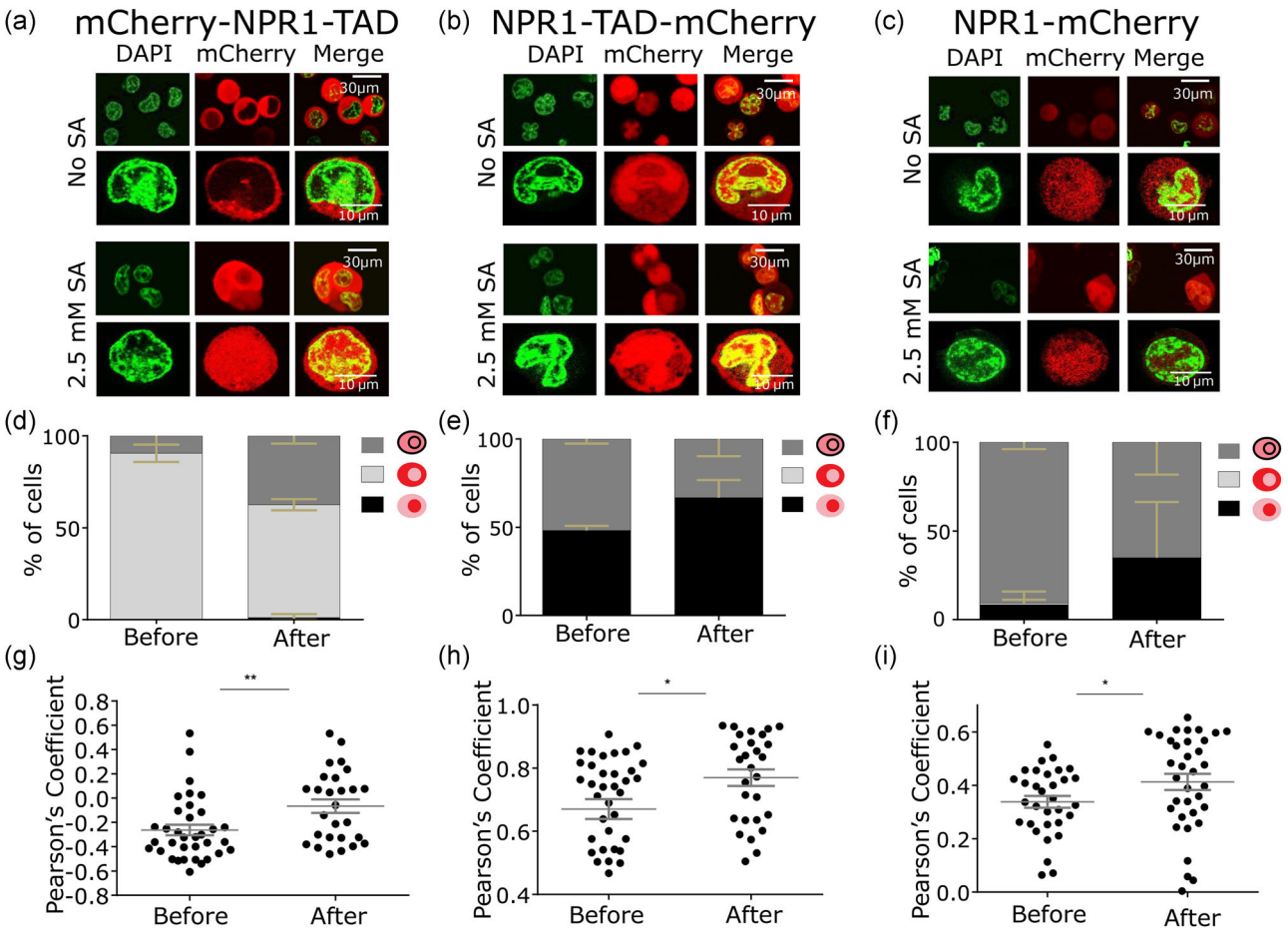

FIGURE 3 SA inducible translocation of mCherry NPR1 fusion proteins. Representative microscopy images of DAPI (nucleus), mCherry, and the merged channels in the absence and presence of 2.5 mM SA for (a) mCherry-NPR1-TAD, (b) NPR1-TAD-mCherry, and (c) NPR1-mCherry confirming SA-dependent translocation of the NPR1 constructs. Bar graphs reporting the percentage of cells with N, C, or D localization for (d) mCherry-NPR1-TAD, (e) NPR1-TAD-mCherry, and (f) NPR1-mCherry. PCC values for the overlap of mCherry with the nucleus for (g) mCherry-NPR1-TAD, (h) NPR1-TAD-mCherry, and (i) NPR1-mCherry. The PCC numbers are computed using JaCop plugin on ImageJ. At least 30 single cells from one of three representative experiments are shown. A *t*-test was used for comparing the two distributions. $^{*}p < 0.05$, and $^{**}p < 0.01$. For panels (d–i), the error bars represent the SEM from three independent experiments

10970290, 2022, 1, Downloaded from https://onlinelibrary.wiley.com/doi/10.1002/bit.27966 by University Of Houston Library Central Campus, Wiley Online Library on [12/02/2023]. See the Terms and Conditions (https://onlinelibrary.wiley.com/terms-and-conditions) on Wiley Online Library for rules of use; OA articles are governed by the applicable Creative Commons License

$p = 0.018$). Similar to the NPR1-TAD-mCherry construct, 100% of HEK cells expressing NPR1-mCherry showed nuclear expression (D & N) of mCherry in the presence or absence of SA (Figure 3c,f,i). 7% of these cells had predominant nuclear localization in the absence of SA and the addition of SA increased this frequency to 41%. Thus, the frequency of cells showing predominant nuclear localization of mCherry increased in the presence of SA and this also led to the significantly increased nuclear colocalization by PCC (Figure 3i; 0.34 ± 0.06 vs. 0.45 ± 0.07; $p = 0.026$). Collectively these results showed that both NPR1 and NPR1-TAD when fused to the N-terminus of mCherry facilitate basal nuclear translocation in the absence of SA but the translocation is significantly increased in response to SA. The major difference between the two constructs was that NPR1-mCherry showed lower nuclear colocalization compared to NPR1-TAD-mCherry both in the presence and absence of SA (Figure 3e,f).

In aggregate, data from all four of these constructs illustrated that regardless of responsiveness to SA, C-terminal NPR1 fusions facilitate cytoplasmic expression (cells are predominantly either C or D) whereas N-terminal NPR1 fusions facilitate nuclear expression (cells are predominantly either N or D).

3.3 | Single-cell SA-dependent protein localization using mesh microarray system

Since we established that three constructs; mCherry-NPR1-TAD, NPR1-TAD-mCherry, and NPR1-mCherry showed translocation of mCherry mediated by SA, we prioritized these for further characterization. We utilized a mesh microarray system to understand the kinetics of translocation at the single-cell level and to enable tracking of the same individual cells. The micromesh array contains nanoliter wells that allowed us to image protein translocation dynamically (Figure 4a).

Cells that stably express mCherry-NPR1-TAD, NPR1-mCherry, and NPR1-TAD-mCherry were loaded on the mesh with 100 μm depth and imaged using a confocal microscope. Cells were imaged 7 and 24 h after the addition of SA (Figure 4b–d). Single-cell tracking experiments confirmed the previously observed behaviors with each of the constructs: cells expressing mCherry-NPR1-TAD transitioned from predominantly cytoplasmic expression (C at 0 h: 88%, C at 7 h: 52%, and C at 24 h: 24%) to more diffuse expression (D at 0 h:12%, D at 7 h: 48%, and D at 24 h: 76%; Figure 4e). These results are also reflected the time-dependent increase in PCC upon addition of SA (Figure 4h). We observed that cells expressing the two N-terminal fusions, NPR1-mCherry, and NPR1-TAD-mCherry, showed an increased frequency of cells expressing mCherry predominantly in the nucleus in response to the addition of SA (Figure 4f,g). This was reflected in a time-dependent increase in PCC upon the addition of SA (Figure 4i,j). The magnitude of protein translocation was most pronounced for mCherry-NPR1-TAD and least for NPR1-TAD-mCherry. Collectively, these results established that the translocation of the NPR1 fusion proteins is completed within 24 h.

3.4 | Reversibility of the NPR1 fusion proteins

After extensively characterizing the SA-mediated nucleocytoplasmic shuttling of mCherry constructs, we next investigated whether removing SA would reverse the nuclear translocation of mCherry. We examined the reversibility of mCherry localization at three stages: (a) basal, before the addition of SA (0 h); (b) induced, at 20 h and 30 h after the addition of SA; and (c) reversed, at 48 h, wherein after 30 h the media containing SA was removed and replaced with SA free media (Figure 5a). After the removal of SA, the cells expressing mCherry-NPR1-TAD transitioned from diffuse (D = 37%, C = 63% at 30 h) to cytoplasmic localization (D = 20%, C = 80% at 48 h; Figure 5b,e). Tracking the PCC confirmed nuclear translocation of mCherry from the basal to the induced states (-0.05 ± 0.005 vs. 0.11 ± 0.01; $p < 0.0001$) and reversal after the withdrawal of SA (Figure 5h; -0.05 ± 0.005 vs. -0.05 ± 0.005).

We observed similar behavior with both constructs expressing NPR1 or NPR1-TAD at the N-terminus. The frequency of cells expressing NPR1-TAD-mCherry displaying predominant nuclear localization increased upon the addition of SA (43%–91%; Figure 5f). Upon the removal of SA, the percentage of cells exhibiting predominant nuclear localization reduced to 64% at 48 h (Figure 5f). This behavior was also captured in the PCC data (Figure 5i; 0.66 ± 0.07 at $t = 0$ h vs. 0.77 ± 0.08 at $t = 30$ h; $p < 0.0001$ and 0.66 ± 0.07 at $t = 0$ h vs. 0.62 ± 0.07 at $t = 48$ h, $p = 0.26$). Although the frequency of cells with predominant nuclear localization was lower with cells expressing NPR1-mCherry compared to NPR1-TAD-mCherry, the inducible and reversible behavior was largely conserved (Figure 5j; 0.29 ± 0.03 at $t = 0$ h vs. 0.43 ± 0.05 at $t = 30$ h; $p < 0.0001$ and 0.29 ± 0.03 at $t = 0$ h vs. 0.31 ± 0.03 at $t = 48$ h, $p = 0.63$). Consistent with our single-cell tracking experiments, protein translocation and reversibility were most pronounced for mCherry-NPR1-TAD and least for NPR1-TAD-mCherry. Collectively, our data suggest that translocation mediated by SA is both inducible and reversible.

4 | DISCUSSION

Ligand-induced translocation of proteins is a versatile tool in biotechnology for applications ranging from understanding tissue-specific conditional expression to adoptive cell therapies. The most well-characterized proteins used for these applications are derived from mammalian proteins and hence the administration of the ligands can cause an off-target response from the activation of endogenous genes. Bacterial-based systems on other hand are both immunogenic and the ligands such as tetracycline and doxycycline can promote antibiotic resistance (Grossman, 2016). There is a compelling need for identifying orthogonal systems that are responsive to small-molecule ligands that are well suited for application in mammals.

We aimed to develop an SA-based inducible protein translocation in mammalian cells. SA is the major metabolite of aspirin, and the safety, pharmacokinetics, and pharmacodynamics have been extensively characterized in humans. To identify SA-based sensors, we

10970290, 2022, 1, Downloaded from https://onlinelibrary.wiley.com/doi/10.1002/bit.27966 by University Of Houston Library Central Campus, Wiley Online Library on [12/02/2023]. See the Terms and Conditions (https://onlinelibrary.wiley.com/terms-and-conditions) on Wiley Online Library for rules of use; OA articles are governed by the applicable Creative Commons License

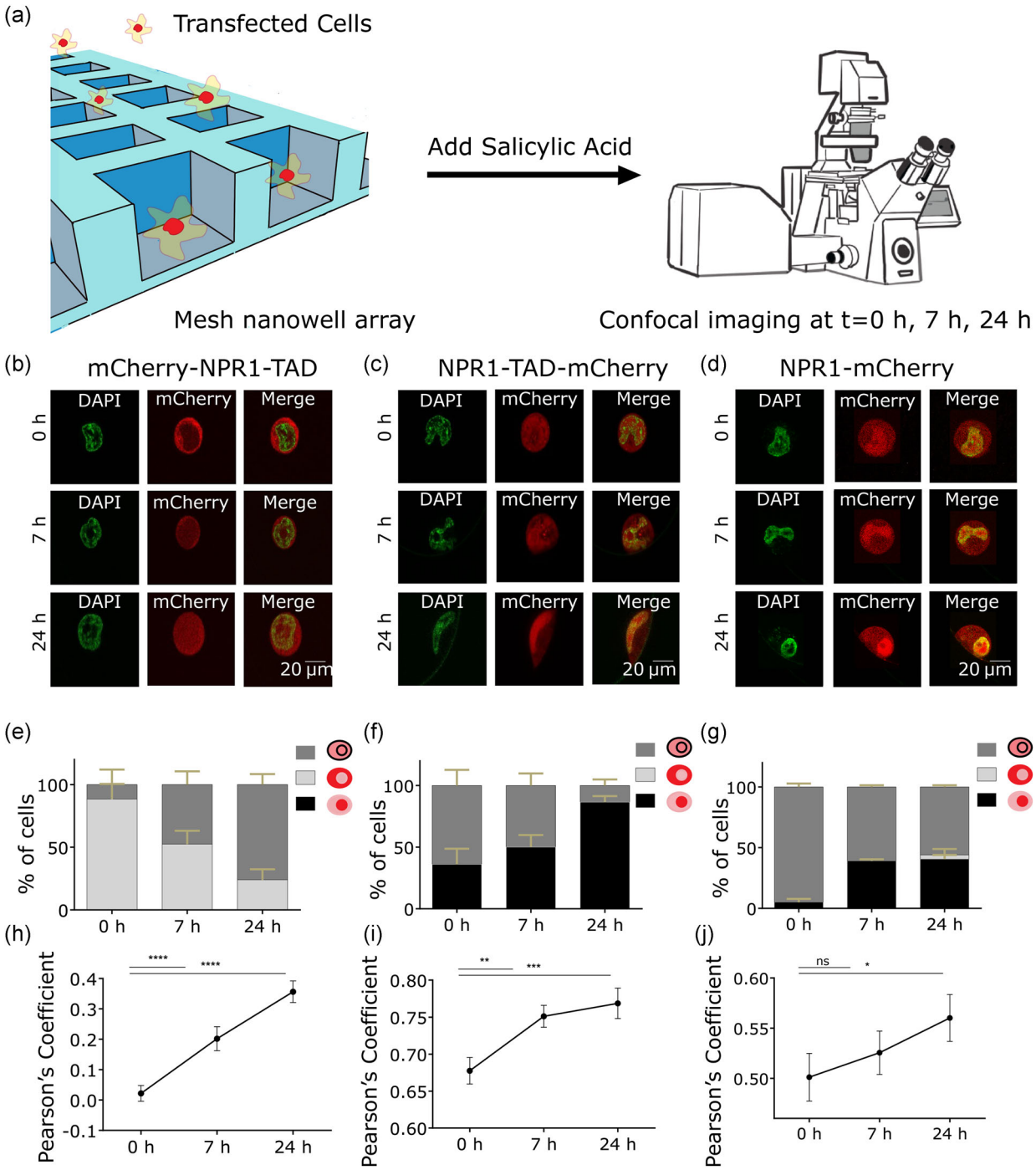

FIGURE 4 Tracking the dynamics of SA-mediated protein translocation at the single-cell level. (a) Illustration of assay procedure including the addition of transfected cells into the nanoliter mesh microarray followed by imaging of individual wells before and after SA treatment. Representative images of DAPI (nucleus), mCherry, and the merged channels of a single cell captured at time 0, 7, and 24 h after SA addition for (b) mCherry-NPR1-TAD, (c) NPR1-TAD-mCherry, and (d) NPR1-mCherry. (e) The percentage of fusion proteins with predominantly cytoplasmic expression decreased in mCherry-NPR1-TAD. Predominantly nuclear localization was increased in (f) NPR1-TAD-mCherry and (g) NPR1-mCherry fusion proteins. Time-dependent increase in PCC was observed in (h) mCherry-NPR1-TAD, (i) NPR1-TAD-mCherry, (j) NPR1-mCherry. The PCC was computed for the overlap of mCherry and the nucleus. ANOVA was used for comparing the distributions. $^{*}p < 0.05$, $^{**}p < 0.01$, $^{***}p < 0.001$, and $^{****}p < 0.0001$. For panels (e–j), the error bars represent the SEM from three independent experiments

10970290, 2022, 1, Downloaded from https://onlinelibrary.wiley.com/doi/10.1002/bit.27966 by University Of Houston Library Central Campus, Wiley Online Library on [12/02/2023]. See the Terms and Conditions (https://onlinelibrary.wiley.com/terms-and-conditions) on Wiley Online Library for rules of use; OA articles are governed by the applicable Creative Commons License

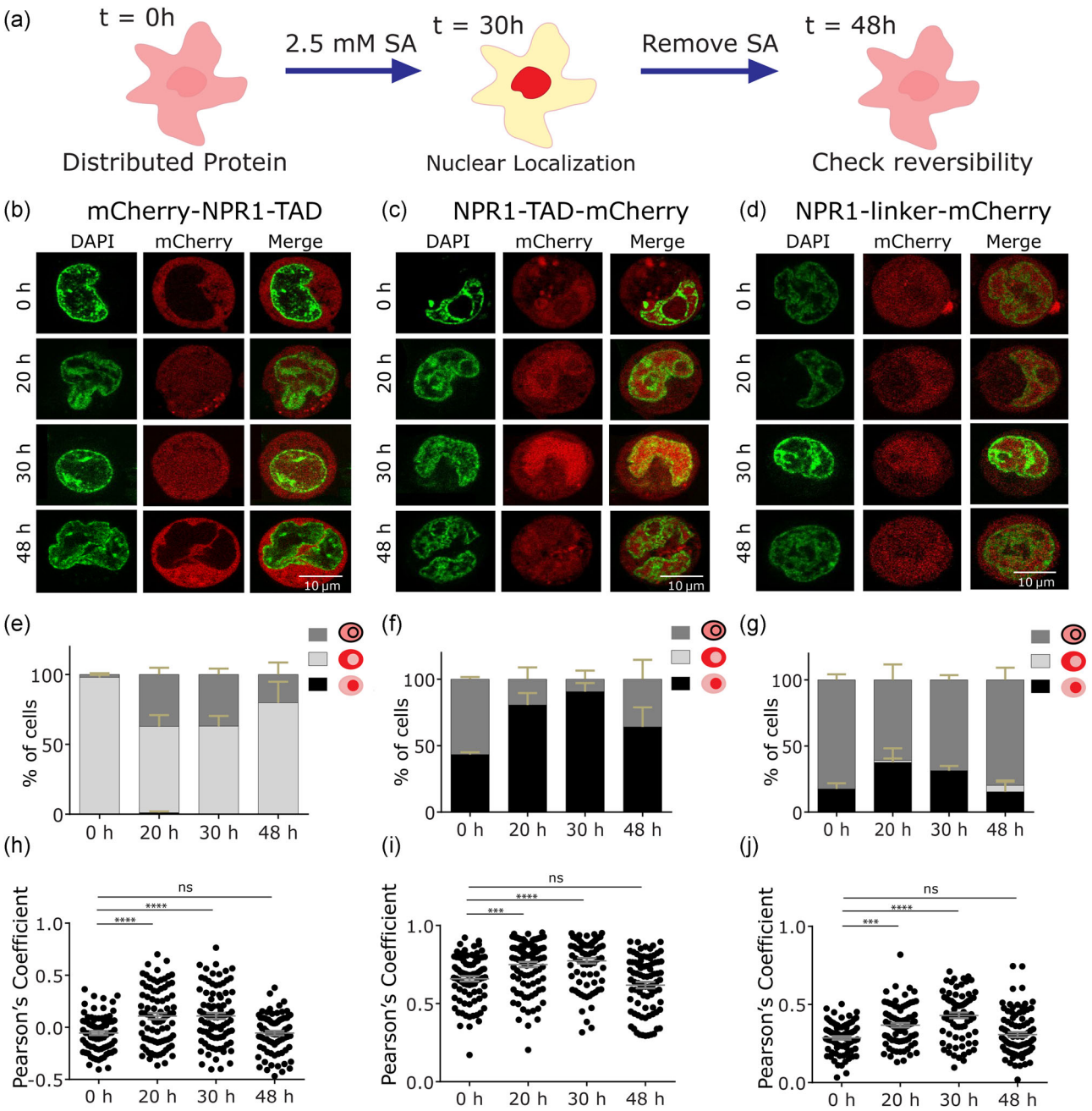

FIGURE 5 SA-mediated translocation of NPR1 fusion proteins is reversible. (a) Reversibility was investigated by treatment of the transfected cells with SA for 30 h followed by withdrawal of SA. Cells were imaged 18 h post removal of SA. Single-cell images of DAPI (nucleus), mCherry, and the merged channels at 0, 20, 30, and 48 h (18 h after removal of SA) of (b) mCherry-NPR1-TAD, (c) NPR1-TAD-mCherry, and (d) NPR1-mCherry. Removal of SA at 48 h led to (e) increase in predominantly cytoplasmic expression in mCherry-NPR1-TAD from 30 to 18 h post removal of SA. Decrease in nuclear localization in (f) NPR1-TAD-mCherry and (g) NPR1-mCherry. The error bars represent the SEM from three independent experiments. Time-dependent increase in PCC was observed in (h) mCherry-NPR1-TAD, (i) NPR1-TAD-mCherry, and (j) NPR1-mCherry. The PCC was computed for the overlap of mCherry and the nucleus. At least 30 single cells from one of two representative experiments are shown. ANOVA was used for comparing the distributions. $^{*}p < 0.05$, $^{**}p < 0.01$, $^{***}p < 0.001$, and $^{****}p < 0.0001$

focused on plants since SA is known to be a hormone essential for innate immunity. Although it is well known that the NPR1/3/4 proteins are sensors of SA, the exact affinity and roles of these different proteins in SA sensing are controversial. *A. thaliana* (At) NPR4 is a high-affinity sensor of SA (K_D = 24 nM) whereas the affinity of NPR1 for SA is 130–200 nM (; Ding et al., 2018; Wu et al., 2012). Comparative studies with both AtNPR1 and *Nicotiana tobacco* NtNPR1 have shown that the N-terminal domains of these proteins (amino acids 1–315) harbor a strong SA inducible transactivation domain (Han, 2019). Both AtNPR1 and NtNPR1 are activated by SA but

10970290, 2022, 1, Downloaded from https://onlinelibrary.wiley.com/doi/10.1002/bit.27966 by University Of Houston Library Central Campus, Wiley Online Library on [12/02/2023]. See the Terms and Conditions (https://onlinelibrary.wiley.com/terms-and-conditions) on Wiley Online Library for rules of use; OA articles are governed by the applicable Creative Commons License

NtNPR1 accumulates predominantly in the nucleus even in the absence of SA (Maier et al., 2011). AtNPR1 on the other hand is present in the cytoplasm (likely in an oligomeric form) and upon the addition of SA undergoes reduction/conformation change exposing a bipartite NLS that facilitates transport to the nucleus. The C-terminal transactivation domain of AtNPR1 (aa 513–593) has been shown to bind directly to SA with a K_D of 1.49 μM (Wu et al., 2012). This however is controversial since the putative SA binding domain of NPR1s is predicted to be the conserved ^{429}LENRV^{433} motif (AtNPR1 numbering; Maier et al., 2011).

To map the SA-mediated translocation domain of AtNPR1, we employed a heterologous expression system using HEK293 cells. This system isolates the SA binding activity of NPR1 and is not subjected to interference from plant defense compounds or signaling cascades. We employed a stable expression system mediated by viral transduction and used mCherry as the live-cell reporter. Our results indicate that the AtNPR1 protein, upon the addition of SA, mediates nuclear translocation in HEK293 mammalian cells without the requirement for any accessory plant-derived proteins. At SA concentrations of 1–2.5 mM, we observed that the TAD of NPR1 was sufficient to render the protein in the nucleus upon the addition of the SA. When NPR1 or NPR1-TAD was fused at the C-terminus of mCherry they showed strong nuclear exclusion but translocation mediated by SA was only accomplished with NPR1-TAD. This suggests that the N-terminus of NPR1, if present, must be free to enable SA responsive translocation. By contrast, when NPR1 or NPR1-TAD was fused at the N-terminus of mCherry both constructs showed SA responsive translocation but also basal nuclear expression in the absence of SA.

With respect to the molecular mechanisms of translocation of NPR1 mediated by SA, our results show that the 80 amino acid TAD can mediate nuclear translocation of passenger proteins in the presence of SA and does not require the interaction with the N-terminus of NPR1 to facilitate translocation. As we show, this property is also reversible upon the withdrawal of SA and the proteins revert to their original localization within the cells. It is important to note that unlike the full-length AtNPR1, the AtNPR1-TAD lacks both Cys82 and Cys216 that have been reported to be essential for oligomer monomer transition and subsequent nuclear localization (Table 1). Second, since mCherry-NPR1-TAD is only ~36 kDa it is anticipated that passive diffusion through the nuclear pores can enable nuclear translocation. Despite this observation, mCherry-NPR1-TAD shows strong nuclear exclusion in the absence of SA (Table 1). We used the NetNES1.1 server for predicting nuclear export signals within full-length At-NPR1 and the program identified the leucine-rich ^{561}LELGNSSL^{568} as a putative NES within the TAD (Cour et al., 2004). Broadly, our results are consistent with the aforementioned study that showed that the TAD can directly bind to SA and advances it further by illustrating that they can mediate SA-induced translocation. At first glance, our results are not consistent with the known SA binding motif of NPR1 and the

TABLE 1 Summary of results obtained from SA-mediated translocation studies in HEK293 cells

Construct	Size (kDa)	Predicted transport	Subcellular localization		SA-mediated change?	NPR1 has a free N or C-term?	Cys82 and Cys216 of NPR1 present?	Reversible?	Comment
			No SA	With SA					
mCherry-NPR1	~93	Active	C = 100 PCC = 0.03	C = 100 PCC = 0.08	No translocation	C	Yes	N/A	Strong nuclear exclusion in the absence of SA: no translocation
mCherry-NPR1-TAD	~36	Passive/active	C = 98 D = 2 PCC = 0.05	C = 63 D = 37 PCC = 0.11	↑Diffuse/nuclear	C	No	Yes C = 80, D = 20 PCC = 0.05	Strong nuclear exclusion in the absence of SA
NPR1-TAD-mCherry	~36	Passive/active	D = 57 N = 43 PCC = 0.66	D = 9 N = 91 PCC = 0.77	↑Nuclear	N	No	Yes N = 64, D = 36 PCC = 0.62	Strong nuclear localization after the addition of SA
NPR1-mCherry	~93	Active	D = 82 N = 18 PCC = 0.29	D = 69 N = 31 PCC = 0.43	↑Nuclear	N	Yes	Yes N = 15, D = 80 PCC = 0.31	Increase in cells with exclusive nuclear localization

Note: C denotes predominant cytoplasmic expression, D denotes diffuse (both cytoplasmic and nuclear), and N denotes predominant nuclear localization.

10970290, 2022, 1, Downloaded from https://onlinelibrary.wiley.com/doi/10.1002/bit.27966 by University Of Houston Library Central Campus, Wiley Online Library on [12/02/2023]. See the Terms and Conditions (https://onlinelibrary.wiley.com/terms-and-conditions) on Wiley Online Library for rules of use; OA articles are governed by the applicable Creative Commons License

recently solved crystal structure of NPR4 bound to SA (Wang et al., 2020). Unlike our results with the TAD, the other studies implicate amino acids 400-500 as the key SA binding regions of NPR1 with Arg432 playing an indispensable role (Hermann et al., 2013; Maier et al., 2011; Wang et al., 2020). A more careful comparison allows us to posit that our results obtained with high concentrations of SA only show that the TAD can mediate nuclear translocation in response to SA but that the true high affinity nanomolar binding region might still be present within amino acids 400–500. As our results with full-length NPR1 illustrate, the presence of the full-length protein does not improve SA mediated nuclear translocation of passenger proteins.

From a biotechnological perspective, the NPR1-TAD is attractive as an SA-mediated nuclear translocator with the best translocator, mCherry-NPR1-TAD performing nuclear translocation as efficiently as widely utilized the estrogen receptor alpha system (Zhao et al., 2018). There are several advantages to this system. The small size of the TAD minimizes the metabolic load of protein expression. Second, since it is of nonmammalian origin, it is likely immunogenic but again the small size decreases the number of available epitopes. Third, since it is not of microbial origin, it is not likely to be compromised by pre-existing immunity (Auslander & Fussenegger, 2016; Gu et al., 2018; Stanton et al., 2014). From an application standpoint, when fused at the C-terminus of the passenger protein, the basal state is strong nuclear exclusion and hence might be appropriate for DNAse based kill switches in adoptive cell therapy or Cas9 based inducible editors. When fused at the N-terminus of the passenger protein, the induced state is strong nuclear localization and hence this might be attractive for transactivation of gene expression. We recognize however that these are conceptual frameworks and our study has only illustrated these behaviors with mCherry. Nonetheless, the availability of small protein domains like the NPR1-TAD that can facilitate SA-mediated nuclear translocation in mammalian cells has strong potential for translational applications within living organisms.

ACKNOWLEDGMENTS

This publication was supported by the NIH (U01AI148118, R01GM143243), CPRIT (RP180466), MRA Established Investigator Award (509800), NSF (1705464), CDMRP (CA160591), and Owens foundation. The authors would like to acknowledge the MDACC Flow Cytometry and Cellular Imaging Core facility for the FACS sorting (NCI P30CA16672).

CONFLICTS OF INTEREST

UH has filed a patent based on some of the technologies in this study.

DATA AVAILABILITY STATEMENT

The data that support the findings of this study are available from the corresponding author upon reasonable request.

ORCID

Navin Varadarajan http://orcid.org/0000-0001-7524-8228

REFERENCES

Auslander, S., & Fussenegger, M. (2016). Engineering gene circuits for mammalian cell-based applications. *Cold Spring Harbor Perspectives in Biology*, *8*, https://doi.org/10.1101/cshperspect.a023895

Chen, X., Zaro, J. L., & Shen, W. C. (2013). Fusion protein linkers: Property, design and functionality. *Advanced Drug Delivery Reviews*, *65*, 1357–1369. https://doi.org/10.1016/j.addr.2012.09.039

la Cour, T., Kiemer, L., Mølgaard, A., Gupta, R., Skriver, K., & Brunak, S. (2004). Analysis and prediction of leucine-rich nuclear export signals. *Protein Engineering, Design & Selection*, *17*(6), 527–536. https://doi.org/10.1093/protein/gzh062

Ding, Y., Sun, T., Ao, K., Peng, Y., Zhang, Y., Li, X., & Zhang, Y. (2018). Opposite roles of salicylic acid receptors NPR1 and NPR3/NPR4 in transcriptional regulation of plant immunity. *Cell*, *173*, e1415–e1467. https://doi.org/10.1016/j.cell.2018.03.044

Feil, R., Brocard, J., Mascrez, B., LeMeur, M., Metzger, D., & Chambon, P. (1996). Ligand-activated site-specific recombination in mice. *Proceedings of the National Academy of Sciences of the United States of America*, *93*, 10887–10890. https://doi.org/10.1073/pnas.93.20.10887

Fu, Z. Q., Yan, S., Saleh, A., Wang, W., Ruble, J., Oka, N., Mohan, R., Spoel, S. H., Tada, Y., Zheng, N., & Dong, X. (2012). NPR3 and NPR4 are receptors for the immune signal salicylic acid in plants. *Nature*, *486*, 228–232. https://doi.org/10.1038/nature11162

Fuhrmann-Benzakein, E., Garcia-Gabay, I., Pepper, M. S., Vassalli, J. D., & Herrera, P. L. (2000). Inducible and irreversible control of gene expression using a single transgene. *Nucleic Acids Research*, *28*, E99. https://doi.org/10.1093/nar/28.23.e99

Grossman, T. H. (2016). Tetracycline antibiotics and resistance. *Cold Spring Harbor Perspectives in Medicine*, *6*, a025387. https://doi.org/10.1101/cshperspect.a025387

Gu, X., He, D., Li, C., Wang, H., & Yang, G. (2018). Development of inducible CD19-CAR T cells with a tet-on system for controlled activity and enhanced clinical safety. *International Journal of Molecular Sciences*, *19*, https://doi.org/10.3390/ijms19113455

Han, G. Z. (2019). Origin and evolution of the plant immune system. *New Phytologist*, *222*, 70–83. https://doi.org/10.1111/nph.15596

Hermann, M., Maier, F., Masroor, A., Hirth, S., Pfitzner, A. J., & Pfitzner, U. M. (2013). The Arabidopsis NIMIN proteins affect NPR1 differentially. *Frontiers of Plant Science*, *4*, 88. https://doi.org/10.3389/fpls.2013.00088

Kelley, L. A., Mezulis, S., Yates, C. M., Wass, M. N., & Sternberg, M. J. (2015). The Phyre2 web portal for protein modeling, prediction and analysis. *Nature Protocols*, *10*, 845–858. https://doi.org/10.1038/nprot.2015.053

Kinkema, M., Fan, W., & Dong, X. (2000). Nuclear localization of NPR1 is required for activation of PR gene expression. *The Plant Cell*, *12*, 2339–2350. https://doi.org/10.1105/tpc.12.12.2339

Liu, E., Tong, Y., Dotti, G., Shaim, H., Savoldo, B., Mukherjee, M., Orange, J., Wan, X., Lu, X., Reynolds, A., Gagea, M., Banerjee, P., Cai, R., Bdaiwi, M. H., Basar, R., Muftuoglu, M., Li, L., Marin, D., Wierda, W., … Rezvani, K. (2018). Cord blood NK cells engineered to express IL-15 and a CD19-targeted CAR show long-term persistence and potent antitumor activity. *Leukemia*, *32*, 520–531. https://doi.org/10.1038/leu.2017.226

Maier, F., Zwicker, S., Hückelhoven, A., Meissner, M., Funk, J., Pfitzner, A. J., & Pfitzner, U. M. (2011). Nonexpressor of pathogenesis-related proteins1 (NPR1) and some NPR1-related proteins are sensitive to salicylic acid. *Molecular Plant Pathology*, *12*, 73–91. https://doi.org/10.1111/j.1364-3703.2010.00653.x

Malamy, J., Carr, J. P., Klessig, D. F., & Raskin, I. (1990). Salicylic acid: A likely endogenous signal in the resistance response of tobacco to viral infection. *Science*, *250*, 1002–1004. https://doi.org/10.1126/science.250.4983.1002

10970290, 2022, 1, Downloaded from https://onlinelibrary.wiley.com/doi/10.1002/bit.27966 by University Of Houston Library Central Campus, Wiley Online Library on [12/02/2023]. See the Terms and Conditions (https://onlinelibrary.wiley.com/terms-and-conditions) on Wiley Online Library for rules of use; OA articles are governed by the applicable Creative Commons License

Métraux, J. P., Signer, H., Ryals, J., Ward, E., Wyss-Benz, M., Gaudin, J., Raschdorf, K., Schmid, E., Blum, W., & Inverardi, B. (1990). Increase in salicylic acid at the onset of systemic acquired resistance in cucumber. *Science*, *250*, 1004–1006. https://doi.org/10.1126/science.250.4983.1004

Reynolds, C. R., Islam, S. A., & Sternberg, M. J. E. (2018). EzMol: A web server wizard for the rapid visualization and image production of protein and nucleic acid structures. *Journal of Molecular Biology*, *430*, 2244–2248. https://doi.org/10.1016/j.jmb.2018.01.013

Rochon, A., Boyle, P., Wignes, T., Fobert, P. R., & Despres, C. (2006). The coactivator function of Arabidopsis NPR1 requires the core of its BTB/POZ domain and the oxidation of C-terminal cysteines. *The Plant Cell*, *18*, 3670–3685. https://doi.org/10.1105/tpc.106.046953

Stanton, B. C., Siciliano, V., Ghodasara, A., Wroblewska, L., Clancy, K., Trefzer, A. C., Chesnut, J. D., Weiss, R., & Voigt, C. A. (2014). Systematic transfer of prokaryotic sensors and circuits to mammalian cells. *ACS Synthetic Biology*, *3*, 880–891. https://doi.org/10.1021/sb5002856

Tada, Y., Spoel, S. H., Pajerowska-Mukhtar, K., Mou, Z., Song, J., Wang, C., Zuo, J., & Dong, X. (2008). Plant immunity requires conformational changes [corrected] of NPR1 via S-nitrosylation and thioredoxins. *Science*, *321*, 952–956. https://doi.org/10.1126/science.1156970

Tsuda, K., Sato, M., Stoddard, T., Glazebrook, J., & Katagiri, F. (2009). Network properties of robust immunity in plants. *PLOS Genetics*, *5*, e1000772. https://doi.org/10.1371/journal.pgen.1000772

Di Ventura, B., & Kuhlman, B. (2016). Go in! Go out! Inducible control of nuclear localization. *Current Opinion in Chemical Biology*, *34*, 62–71. https://doi.org/10.1016/j.cbpa.2016.06.009

Wang, W., Withers, J., Li, H., Zwack, P. J., Rusnac, D. V., Shi, H., Liu, L., Yan, S., Hinds, T. R., Guttman, M., Dong, X., & Zheng, N. (2020). Structural basis of salicylic acid perception by Arabidopsis NPR proteins. *Nature*, *586*, 311–316. https://doi.org/10.1038/s41586-020-2596-y

Wu, Y., Zhang, D., Chu, J. Y., Boyle, P., Wang, Y., Brindle, I. D., De Luca, V., & Després, C. (2012). The Arabidopsis NPR1 protein is a receptor for the plant defense hormone salicylic acid. *Cell Reports*, *1*, 639–647. https://doi.org/10.1016/j.celrep.2012.05.008

Xu, T., Johnson, C. A., Gestwicki, J. E., & Kumar, A. (2010). Conditionally controlling nuclear trafficking in yeast by chemical-induced protein dimerization. *Nature Protocols*, *5*, 1831–1843. https://doi.org/10.1038/nprot.2010.141

Zhang, J., Chen, L., & Wang, Y. (2019). Drug inducible CRISPR/Cas systems. *Computational and Structural Biotechnology Journal*, *17*, 1171–1177. https://doi.org/10.1016/j.csbj.2019.07.015

Zhao, C., Zhao, Y., Zhang, J., Lu, J., Chen, L., Zhang, Y., Ying, Y., Xu, J., Wei, S., & Wang, Y. (2018). HIT-Cas9: A CRISPR/Cas9 genome-editing device under tight and effective drug control. *Molecular Therapy. Nucleic Acids*, *13*, 208–219. https://doi.org/10.1016/j.omtn.2018.08.022

SUPPORTING INFORMATION

Additional supporting information may be found in the online version of the article at the publisher's website.

How to cite this article: Sadeghi, F., Kumar, M., Bandey, I. N., Li, X., Roysam, B., & Varadarajan, N. (2022). Salicylic acid inducible nucleocytoplasmic shuttling of NPR1 fusion proteins in human cells. *Biotechnology and Bioengineering*, 119, 199–210. https://doi.org/10.1002/bit.27966

10970290, 2022, 1, Downloaded from https://onlinelibrary.wiley.com/doi/10.1002/bit.27966 by University Of Houston Library Central Campus, Wiley Online Library on [12/02/2023]. See the Terms and Conditions (https://onlinelibrary.wiley.com/terms-and-conditions) on Wiley Online Library for rules of use; OA articles are governed by the applicable Creative Commons License